

# Decoupled Integral LQR Controller with Anti-windup Compensator for MIMO Two Rotor Aerodynamical System (TRAS)

SAEED AL-HADDAD  
Universiti Teknologi Malaysia  
Faculty of Electrical Engineering  
81310 Johor Bahru, Johor  
MALAYSIA  
sssash88@gmail.com

HERMAN WAHID  
Universiti Teknologi Malaysia  
Faculty of Electrical Engineering  
81310 Johor Bahru, Johor  
MALAYSIA  
herman@fke.utm.my

*Abstract:* This paper employs a design of two sub-controllers based on Linear Quadratic Regulator (LQR) for Two Rotor Aero-dynamical System (TRAS) in two degree of freedom (2-DOF) motion. Two Rotor Aero-dynamical System (TRAS) is a nonlinear multi-input multi-output (MIMO) system with strong cross coupling. The main focus of the research work is to control both the horizontal and vertical angles of the system so that the desired trajectory is tracked while rejecting disturbances. In this work, TRAS is decoupled into two subsystems (horizontal and vertical) and the derivation of the linear model of each subsystem is developed using Jacobean linearisation matrix. Optimal LQR controller is designed and tuned using Particle Swarm Optimisation (PSO) algorithm for each subsystem. The designed sub-LQR controllers are combined with integral action gain, full state observe and an anti-integral windup based on back-calculation technique. Simulation results show that the decoupled integral LQR controller (DILQRC) exhibits a better performance in terms of transient and steady state responses with significant reduction of settling time, overshoot percentage and error index it also requires less and smooth control signal in case of tracking a step input as compared to the cross coupled PID controller (CCPIDC). Furthermore, a successful experimental validation is demonstrated to emphasise the effectiveness of the proposed control method.

*Key-Words:* Two Rotor Aerodynamical System (TRAS), Linear Quadratic Regulator (LQR), integral action gain, Particle Swarm Optimisation (PSO), full state observer, anti-windup, back-calculation.

## 1 Introduction

Control of two rotor aerodynamical system (TRAS) has become one of the most challenging engineering tasks due to the complicated nonlinear interaction and significant cross-coupling between the horizontal and vertical planes. Furthermore, some state variables are not accessible for measurement.

Fractional order PID controller using Nelder-Mead optimisation technique was able to minimise the cross coupling between the system planes also it required less control effort to stabilise the system as compared to other classical PID controllers [1]. On the other side, the system has a settling time above 9 seconds for both horizontal and vertical angles of the system as well as a high percentage of overshoot above 13% for both angles. A composite controller of active disturbance rejection and input shaping command has been investigated in simulation and real time implementation as reported in [2]. However, both angles of the system have a settling time of more than 6.3 seconds and 9.1

seconds in simulation and experimental results, respectively. Fixed structure  $H_\infty$  controller with static linear decoupling method is found to be capable of handling the system effectively because of its simple structure and robust nature as proposed in [3].

In [4], an optimal tuned Linear Quadratic Regulator (LQR) controllers have shown good results to control and stabilise the system for each horizontal and vertical planes with magnificent reduction in settling time and overshoot percentage, but the controllers were only implemented in simulation for one degree of freedom (1-DOF) motion and the robustness of the system was not investigated. Optimal LQR controller with integral action gave better performance as compared to the sliding mode controller [5] and an optimal LQR controller is found to provide a better performance with reduced control effort as compared to the classical PID controller [6]. Nevertheless, both studies show that the system has a settling time above 5 seconds for both angles and no conclusions were drawn on the system robustness properties.

Wen and Lu [7] experimentally validated the use of robust deadbeat control technique for the twin rotor MIMO system in 2-DOF, however, the vertical angle takes about 8 seconds to be settled with a small percentage of overshoot in the horizontal angle. Simulation and experimental results of Multiple models with second level adaption controller showed improvement in transient and steady responses in comparison with single model adaptive controller [8]. However, the simulation results shows that the system settles in less than 7 seconds for both angles, meanwhile, that performance significantly degraded in the real-time implementation as the system takes more than 12 seconds to be settled for both angles with 35.6% of overshoot in the vertical angle.

A multivariable integral sliding mode controller has been used to track both the azimuth and pitch angles of the system and it showed excellent tracking behaviour for both angles with small errors [9]. In [10], a nonlinear model predictive controller (MPC) with extended Kalman filter is validated experimentally to have a superior performance as compared to multivariable PID controller, in spite of that, the tuning of the large number of MPC parameters was the most time consuming problem in this study. MIMO model predictive controller is found to be capable of handling the cross coupling between the system parameters while rejecting disturbances and maintains robustness to the system as reported in [11]. However, the system is able to track the reference trajectories with a settling time less than 20 seconds and a percentage of overshoot less than 7.5% for both angles, moreover, the system is subjected to a number of oscillations due to the gravity effect.

It can be concluded that the control of TRAS system is divided into two main categories: the linear and nonlinear controllers. The linear controllers have a simple structure and lower computational cost but they are suffering from long settling time and a higher percentage of overshoot. On the other hand, the nonlinear controllers have a superior performance and robust nature but they involve a higher computational cost and difficulties in real time implementation, especially those who are involved adaption laws that significantly increase the computational load and deteriorate the transient response when the adaption is initiated [12].

The main contribution of this work, is the designing of two linear sub-controllers based on optimal tuned LQR controller with integral action for TRAS system in 2-DOF that have a simple structure, low computational cost and faster tracking response with small percentage of overshoot as compared to other controller design techniques presented in the literature.

In this work, TRAS is decoupled into two subsystems (horizontal and vertical) and the derivation of the linear model of each subsystem is developed using Jacobean linearisation matrix. Optimal LQR controller is designed and tuned using Particle Swarm Optimisation (PSO) algorithm for each subsystem with the addition of integral action. Full state observer based on Luenberger observer is designed for each subsystem in order to estimate the states of the system. Furthermore, an anti-integral windup technique based on back-calculation is implemented for each sub-controller. The evaluation of the designed controller is based on set point tracking and disturbance rejection, and in order to provide a point of comparison the performance of the designed controller is compared to the existing cross coupled PID controller (CCPIDC) tuned by the manufacturer.

The remainder of this paper is organised as follows: Section 2 describes the linear and nonlinear models of TRAS system. In section 3, an optimal LQR controller with integral action is presented. The principles of PSO algorithm is illustrated in section 4, followed by the design of full state observer in section 5. Section 6, shows the design of an anti-integral windup technique based on back-calculation. Stability analysis of closed loop subsystems are carried out in section 7. Simulation and experimental result are deliberated in Sections 8 and 9, respectively followed by the concluding remarks in section 10.

## 2 TRAS Description and Modelling

The two rotor Aero-dynamical system (TRAS) is a multivariable system that has two inputs and two outputs with significant interaction between its parameters. TRAS is a laboratory setup that is used to test and validate various flight control methods as it resembles the behaviour of helicopter in certain aspects as shown in Figure 1. The TRAS model description and physical parameters are provided in Table 1 [13].

However, in a typical helicopter, the aerodynamic force is controlled by changing the angle of attack of the blades while in laboratory setup, it is constructed such that the angle of attack of the blades is fixed and the controlling is done by varying the rotational speed of the rotors. The TRAS consists of two rotors which are the main and tail rotors. Both rotors are driven by two direct current (DC) motors, the main rotor is used to control the vertical motion (pitch angle) and the tail rotor is used to control the horizontal motion (azimuth angle). Two counterbalance levers attached with a weight

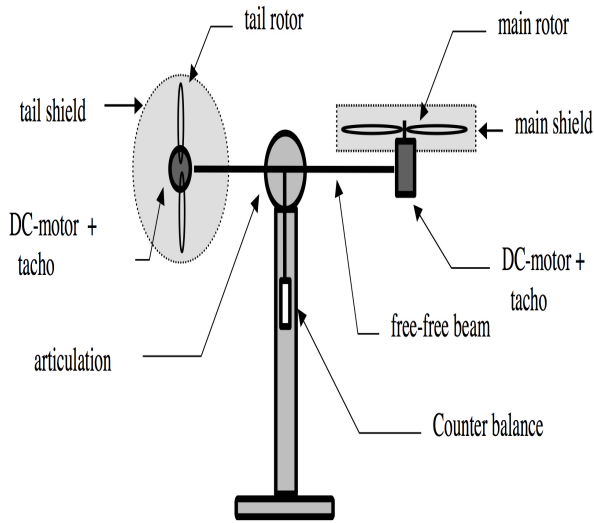


Fig. 1 TRAS system [13].

at their ends are fixed to the beam at the pivot that determines the steady-state pitch angle [13].

## 2.1 Nonlinear Models

The mathematical modelling of the horizontal plane can be written as in Eq. 1 to Eq. 3 [13]:

$$\dot{x}_1 = \frac{1}{J_h} x_2 \quad (1)$$

$$\dot{x}_2 = \frac{l_t F_h(x_3)}{I_h} - \frac{k_h}{J_h} x_2 + \frac{a_1}{J_h \times I_h} x_2 |x_3| \quad (2)$$

$$\dot{x}_3 = u_h - \frac{u_h(x_3)}{I_h} \quad (3)$$

where:

$$F_h(x_3) \cong -4.869 \times 10^{-20} x_3^5 - 5.035 \times 10^{-17} x_3^4 + 4.64 \times 10^{-12} x_3^3 + 7.562 \times 10^{-9} x_3^2 + 2.435 \times 10^{-5} x_3 - 0.003716 \quad (4)$$

$$u_h(x_3) \cong -1.08 \times 10^{-20} x_3^5 + 5.25 \times 10^{-18} x_3^4 + 1.43 \times 10^{-12} x_3^3 - 8.13 \times 10^{-10} x_3^2 + 0.0001534 x_3 + 0.002067 \quad (5)$$

where:  $x_1$  is the azimuth angle,  $x_2$  is the azimuth angular velocity,  $x_3$  is the rotational speed of the tail rotor,

$u_h$  is the control input to the tail rotor,  $F_h(x_3)$  is a nonlinear relationship between the rotational speed of the tail rotor and horizontal thrust and  $u_h(x_3)$  is a nonlinear relationship between the rotational speed of the tail rotor and the control input to the tail rotor.

The mathematical modelling of the vertical plane can be written as in Eq. 6 to Eq. 8 [13]:

$$\dot{x}_4 = \frac{1}{J_v} x_5 \quad (6)$$

$$\dot{x}_5 = \frac{l_m F_v(x_6)}{I_v} - \frac{k_v}{J_v} x_5 - \frac{a_2 k_v}{J_v \times I_v} x_5 |x_6| + g((A - B) \cos x_4 + C \sin x_4) \quad (7)$$

$$\dot{x}_6 = u_v - \frac{u_v(x_6)}{I_v} \quad (8)$$

where:

$$F_v(x_6) \cong -1.345 \times 10^{-18} x_6^5 - 5.221 \times 10^{-16} x_6^4 + 3.513 \times 10^{-11} x_6^3 + 2.17 \times 10^{-18} x_6^2 + 0.0002012 x_6 - 0.01453 \quad (9)$$

$$u_v(x_6) \cong -1.1 \times 10^{-18} x_6^5 + 1.522 \times 10^{-16} x_6^4 - 8.796 \times 10^{-12} x_6^3 - 1.46 \times 10^{-9} x_6^2 + 0.00021664 x_6 - 0.003139 \quad (10)$$

where:  $x_4$  is the pitch angle,  $x_5$  is the pitch angular velocity,  $x_6$  is the rotational speed of the main rotor,  $u_v$  is the control input to the main rotor,  $F_v(x_6)$  is a nonlinear relationship between the rotational speed of the main rotor and vertical thrust and  $u_v(x_6)$  is a nonlinear relationship between the rotational speed of the main rotor and the control input to the main rotor.

## 2.2 Linear Models

The LQR controller is a linear state feedback controller which requires a linear model to be implemented, thus each nonlinear subsystem is linearised using Jacobean linearisation matrix around the equilibrium point  $(x, u)$  at  $(0, 0)$  [14]. Where  $x$  is the states of each subsystem and  $u$  is the control input. The  $A$  and  $B$  Jacobean linearisation matrices for each subsystem can be evaluated as follows [14]:

$$A = \left. \frac{\partial f}{\partial x} \right|_{x=0, u=0}; B = \left. \frac{\partial f}{\partial u} \right|_{x=0, u=0}$$

**Table 1** Parameters definition of TRAS [13].

| Symbol | Description                                       | Value                                    |
|--------|---------------------------------------------------|------------------------------------------|
| $l_t$  | The length of the tail rotor                      | 0.216 m                                  |
| $l_m$  | The length of the main rotor                      | 0.202 m                                  |
| $k_h$  | Friction constant of the tail propeller           | 0.00589                                  |
| $k_v$  | Friction constant of the main propeller           | 0.01271                                  |
| $J_h$  | Moment of inertia with respect to vertical axis   | 0.02683 kgm <sup>2</sup>                 |
| $J_v$  | Moment of inertia with respect to horizontal axis | 0.0300571 kgm <sup>2</sup>               |
| $I_h$  | Moment of inertia for the tail rotor              | $2.7027 \times 10^{-5}$ kgm <sup>2</sup> |
| $I_v$  | Moment of inertia for the main rotor              | $1.64 \times 10^{-4}$ kgm <sup>2</sup>   |
| $a_1$  | Mechanical constant                               | $3.3 \times 10^{-6}$                     |
| $a_2$  | Mechanical constant                               | $9.28 \times 10^{-6}$                    |
| $A$    | Mechanical constant                               | 0.0947                                   |
| $B$    | Mechanical constant                               | 0.04465                                  |
| $C$    | Mechanical constant                               | $9.54136 \times 10^{-3}$                 |
| $g$    | Gravitational acceleration                        | 9.81 ms <sup>-2</sup>                    |

where:  $f$  is the differential equation of each state.

The linear model of each subsystem can be obtained by evaluating the Jacobean linearisation matrices, choosing the azimuth and pitch angles as the output states for the  $C$  matrix of the horizontal and vertical subsystems, respectively and assumes zero feedforward  $D$  matrix for each subsystem.

The linear model of the horizontal plane can be written in state space form as in Eq. 11:

$$\begin{bmatrix} \dot{x}_1 \\ \dot{x}_2 \\ \dot{x}_3 \end{bmatrix} = \begin{bmatrix} 0 & 37.27 & 0 \\ 0 & -0.22 & 0.195 \\ 0 & 0 & -5.68 \end{bmatrix} \begin{bmatrix} x_1 \\ x_2 \\ x_3 \end{bmatrix} + \begin{bmatrix} 0 \\ 0 \\ 1 \end{bmatrix} [u_h]$$

$$y_h = [1 \ 0 \ 0] \begin{bmatrix} x_1 \\ x_2 \\ x_3 \end{bmatrix} + [0] [u_h]$$
(11)

The linear model of the vertical plane can be written in state space form as in Eq. 12:

$$\begin{bmatrix} \dot{x}_4 \\ \dot{x}_5 \\ \dot{x}_6 \end{bmatrix} = \begin{bmatrix} 0 & 33.27 & 0 \\ -0.10 & -0.42 & 0.25 \\ 0 & 0 & -1.42 \end{bmatrix} \begin{bmatrix} x_4 \\ x_5 \\ x_6 \end{bmatrix} + \begin{bmatrix} 0 \\ 0 \\ 1 \end{bmatrix} [u_v]$$

$$y_v = [1 \ 0 \ 0] \begin{bmatrix} x_4 \\ x_5 \\ x_6 \end{bmatrix} + [0] [u_v]$$
(12)

### 3 LQR Controller with Integral Action Gain

By considering a linear time invariant system, the state and output equations with control input can be written

as in Eq. 13 and Eq. 14, respectively [15]:

$$\dot{x} = Ax + Bu \quad (13)$$

$$y = Cx \quad (14)$$

The conventional LQR design problem is to minimise the following quadratic performance index function as in Eq. 15 [16]:

$$J = \int_0^{\infty} (x^T Q x + u^T R u) dt \quad (15)$$

The control input here is linear and the control penalty is given by  $(u^T R u)$  where  $R \in \mathfrak{R}^{m \times m}$  is the square positive definite matrix. The state penalty is expressed as  $(x^T Q x)$  where  $Q \in \mathfrak{R}^{n \times n}$  is a positive semi-definite matrix. The control value  $u$  is representing the optimal control input, which is given by Eq. 16 [16]:

$$u(t) = -Kx(t) = -R^{-1}B^T P x(t) \quad (16)$$

The matrix  $K$  is determined to minimise the performance index. Here,  $P$  is the solution of Riccati equation, and  $K$  is the linear optimal feedback matrix. Riccati equation can be solved by Eq. 17 [16]:

$$PA + A^T P - PBR^{-1}B^T P + Q = 0 \quad (17)$$

The  $Q$  and  $R$  matrices plays an important role on the overall system performance, thus they should be chosen appropriately.

By adding an integral action, a new state that is multi dimensional will be added to the original states of the system [15].

Then the system has the state vector  $[x \ x_a]^T$ , where  $x_a$  is the new integral state, thus we have [15]:

$$\dot{x}_a = r - y = r - Cx \quad (18)$$

$$u = [-K \ K_e] \begin{bmatrix} x \\ x_a \end{bmatrix} \quad (19)$$

where:  $r$  is the reference signal and  $K_e$  is the integral action gain.

By substituting Eq. 18 and Eq. 19 in Eq. 17 and Eq. 16 yields [15]:

$$\begin{bmatrix} \dot{x} \\ \dot{x}_a \end{bmatrix} = \begin{bmatrix} A - BK & BK_e \\ -C & 0 \end{bmatrix} \begin{bmatrix} x \\ x_a \end{bmatrix} + \begin{bmatrix} 0 \\ 1 \end{bmatrix} r \quad (20)$$

$$y = [C \ 0] \begin{bmatrix} x \\ x_a \end{bmatrix} \quad (21)$$

The state space representation of the state feedback control with integral action is shown in Eq. 20 and Eq. 21. By choosing appropriate state feedback gain and integral action gain that makes the system asymptotically stable, the system output will accurately track the reference signal [14].

## 4 Particle Swarm Optimisation (PSO)

PSO optimisation technique was originally inspired by the behaviour of fish swarms, as well as bees and other species [17]. The concept in this technique is to look for the best solution among the whole swarm for a specific cost function. PSO was introduced by James Kennedy and Russell Eberhart in (1995) and it is used as a powerful optimisation algorithm in many applications for its satisfactory results.

Implementing PSO is very simple as only two equations are required for the optimisation process: position equation and velocity equation. For each step in PSO, all particles will be initialised with a random position and velocity vectors and they will be evaluated to a cost function relevant to their position. Similar to most optimisation techniques finding Personal Best  $x_{PB}$  and Global Best  $x_{GB}$  for all particles in each iteration step will be calculated and the position and velocity vectors of each particle will be updated according to Eq. 22 and Eq. 23 [17]:

$$v_i(t+1) = w \times v_i(t) + c_1 \times r_1 \times (x_{PB} - x_i(t)) + c_2 \times r_2 \times (x_{GB} - x_i(t)) \quad (22)$$

$$x_i(t+1) = x_i(t) + v_i(t+1) \quad (23)$$

where:  $w$  is the inertia weight factor,  $c_1$  and  $c_2$  are the personal acceleration coefficient and social acceleration coefficient, respectively and  $r_1$  and  $r_2$  are randomly distributed numbers between (0, 1). The parameter  $w$  makes the particles converge to global best solution rather than oscillating around it.

The optimisation processes are carried out for the tuning of  $Q$  and  $R$  matrices of each LQR sub-controller. Each optimisation process is carried out for 100 iterations. The cost function used in the tuning process is the minimisation of settling time and percentage of overshoot as in Eq. 24:

$$F = ST + OV \quad (24)$$

where:  $ST$  is the settling time and  $OV$  is the percentage of overshoot.

Figure 2 shows the convergence of the cost function for each optimisation process for both the horizontal and vertical sub-controllers parameters tuning. It can be clearly noticed that the particles of PSO is able to find the best solution in almost forty number of iterations. Table 2 shows the result from each optimisation process.

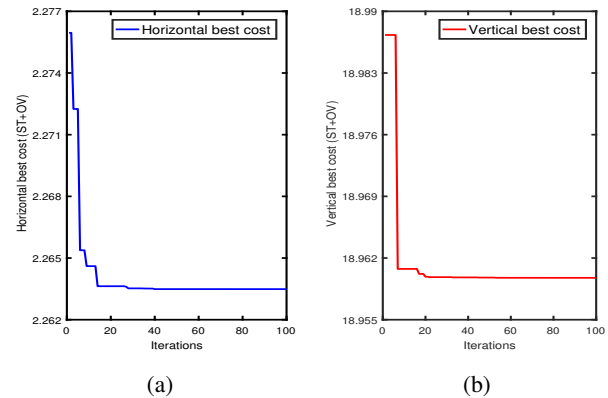


Fig. 2 The convergence of PSO cost function. (a) Horizontal controller best cost, (b) Vertical controller best cost.

**Table 2** Results of PSO algorithm for each sub-controller parameter's tuning.

| Sub-controller | $Q$ matrix                                                                | $R$ matrix |
|----------------|---------------------------------------------------------------------------|------------|
| Horizontal     | $\begin{bmatrix} 538.93 & 0 & 0 \\ 0 & 0 & 0 \\ 0 & 0 & 0 \end{bmatrix}$  | $[ 0.94 ]$ |
| Vertical       | $\begin{bmatrix} 6097.30 & 0 & 0 \\ 0 & 0 & 0 \\ 0 & 0 & 0 \end{bmatrix}$ | $[ 0.16 ]$ |

## 5 Full State Observer

LQR controller requires that all states of the system are available for measurement [18]. For each subsystem there are three state variables, whereas only two are accessible for measurement. Thus a full state observer is designed for each subsystem.

The mathematical model of the observer for linear time invariant system (LTI) can be defined as in Eq. 25 [18]:

$$\dot{\hat{x}} = A\hat{x} + Bu + L(y - C\hat{x}) \quad (25)$$

Since the system is controlled by the estimated feedback, the control input can be written as in Eq. 26 :

$$u = -K\hat{x} + K_e x_a \quad (26)$$

The estimated states can be written as in Eq. 27:

$$\dot{\hat{x}} = A\hat{x} + B(-K\hat{x} + K_e x_a) + L(Cx - C\hat{x}) \quad (27)$$

and it can be arranged as in Eq. 28:

$$\dot{\hat{x}} = (A - LC - BK)\hat{x} + LCx + BK_e x_a \quad (28)$$

The inputs to the observer are the output  $y$  and the control input  $u$ . The gain  $L$  is called the observer gain and it is used as a correction for the model. Chosen of appropriate observer gain value determine how fast the error between the actual and estimated states will converge to zero [18].

As a rule of thumb the observer poles determined by the matrix  $(A - LC - BK)$  should be chosen to be two to five times faster than the controller poles to make sure that the error of the observer converges to zero very fast. However, if the output signal is contaminated by disturbances and measurement noises then the observer poles should be chosen to be slower than the controller poles, so that the bandwidth of the system will become lower and smooth the noise [18].

The horizontal observer poles are chosen to be five times faster than the horizontal controller poles. On the other side, the vertical observer poles are chosen to be four times slower than the vertical controller poles due to the vibrations that occur to the presence of rotor load, motor torque [19] and measurement noise which result in a number of oscillation in the system response with long settling time.

To demonstrate the effect of the vertical observer poles selection on the overall vertical controller performance, the vertical plane is subjected to sinusoidal signal with a measurement noise of a distributed random sequence with noise power of  $0.1 \times 10^{-6}$  as shown in

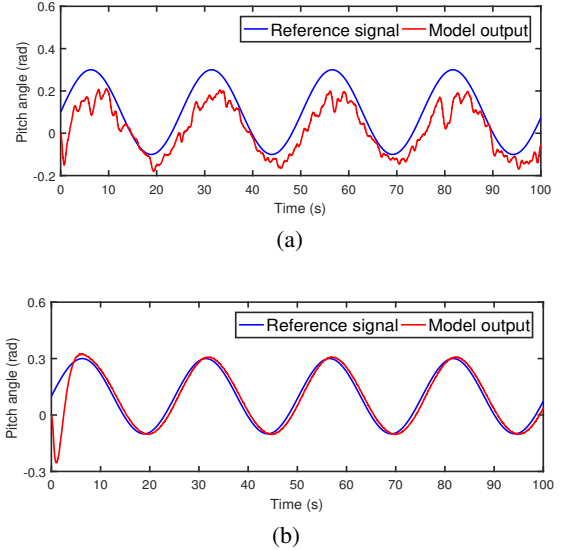


Fig. 3 The effect of observer poles selection on the vertical controller performance. (a) Model output with five times faster observer poles, (b) Model output with four times slower observer poles.

Figure 3. It can be clearly observed that the the output of the vertical plane deviates significantly from the reference signal when the observer poles are five times faster than the controller poles, while in case if the observer poles are four times slower than the controller poles the controller is able to smooth the noise and track the reference signal.

The closed loop of each subsystem with state feedback controller, integral action gain and full state observer can be written in state space form as in Eq. 29:

$$\begin{bmatrix} \dot{x} \\ \dot{x}_a \\ \dot{\hat{x}} \end{bmatrix} = \begin{bmatrix} A & BK_e & -BK \\ -C & 0 & 0 \\ LC & BK_e & A - LC - BK \end{bmatrix} \begin{bmatrix} x \\ x_a \\ \hat{x} \end{bmatrix} + \begin{bmatrix} 0 \\ 1 \\ 0 \end{bmatrix} r \quad (29)$$

$$y = \begin{bmatrix} C & 0 & 0 \end{bmatrix} \begin{bmatrix} x \\ x_a \\ \hat{x} \end{bmatrix}$$

The overall performance of each controller is influenced by the eigenvalues of the state space in Eq. 29, thus they should be placed appropriately to ensure the stability of whole system.

## 6 Anti-integral Windup Compensator (Back-calculation)

In practice all control loops and processes contain nonlinearities such as saturation in actuators. One of the most well known phenomena in control system is the integrator windup especially when the system starts up [20]. Back-calculation technique is based on recomputing the integral term when the controller reaches its limits. In particular, the integral value is increased or decreased by feeding the error signal that produced from the difference between the saturated and unsaturated control signal to the integral action state [20].

Since the linear controller is designed to operate within a linear range, ignoring the actuator nonlinearities will cause the integrator to windup which will significantly deteriorate the closed loop performance. This performance deterioration, is in the form of large overshoot and long settling time [21]. For TRAS system the control signals for the main and tail motors are normalised and change in the range  $[-1,+1]$  which corresponds to a voltage range of  $[-24V,+24V]$ .

In back-calculation technique the difference between the saturated control signal and unsaturated control signal is fed back to the integral action state, thus the new integral action state can be written as follows:

$$\dot{\hat{x}}_a = r - y + (\bar{u} - u) \quad (30)$$

$$\dot{\hat{x}}_a = e + (\bar{u} - u) \quad (31)$$

where:  $e$  is the difference between the reference signal and the measured output.

The controller input for each subsystem with the addition of back-calculation is modified in time domain as in Eq. 32:

$$u = -K\hat{x} + K_e \int_0^t (e + (\bar{u} - u))dt \quad (32)$$

Rewriting the control input equation in Laplace domain as follows:

$$u = -K\hat{x} + \frac{K_e}{s}e + \frac{K_e}{s}(\bar{u} - u) \quad (33)$$

where the saturation function  $sat$  is defined as in Eq. 34 and Eq. 35:

$$\bar{u} = sat(u) \quad (34)$$

$$\bar{u} = \begin{cases} u_{min} & if & u < u_{min} \\ u & if & u_{min} \leq u \leq u_{max} \\ u_{max} & if & u > u_{max} \end{cases} \quad (35)$$

When the actuator saturates, the feedback signal  $(\bar{u} - u)$  attempts to drive the error between the saturated and unsaturated control signals to zero by recomputing the integral action state such that the controller output is exactly at the saturation limit. When there is no saturation, the difference between  $\bar{u}$  and  $u$  will be equal to zero, which breaks the feedback loop of back-calculation, in this case the controller performs as in standard mode ( $u = \bar{u}$ ).

When the actuator saturates  $u$  is different from  $\bar{u}$ . Since the controller is not aware of the saturation in the actuator it computes the states as if the system input is  $u$ , therefore state estimation errors can be alleviated simply by feeding  $\bar{u}$  to each observer instead of  $u$  [22]. The closed loop system under the proposed DILQRC with full state observer and back-calculation technique is shown in Figure 4.

## 7 Stability Analysis of Closed Loop Subsystems

After the designing of the sub-LQR controllers combined with integral action gain, full state observer and back-calculation anti-integral windup technique, the closed loop analysis was carried out before the implementation on the 2-DOF nonlinear TRAS model and real TRAS system.

Frequency response of each closed loop subsystem with linear and nonlinear models is estimated using linear analysis tool in MATLAB/Simulink for the frequencies from 0.01 rad/s to 100 rad/s. Figure 5 Shows the estimated frequency response of each closed loop subsystem. The average estimated bandwidths is approximately 1.43 rad/s and 1.35 rad/s for the horizontal and vertical closed loop subsystems, respectively. The vertical bandwidth is slightly lower than the horizontal bandwidth, this would yield the vertical controller to attenuate and smooth more exogenous disturbance or measurement noise signals that may enter the system. Both horizontal and vertical closed loop subsystems have a gain margin of approximately 14 dB and 15 dB, respectively and phase margin of roughly  $175^\circ$  and  $151^\circ$ , respectively, which indicates that each closed loop subsystem is asymptotically stable.

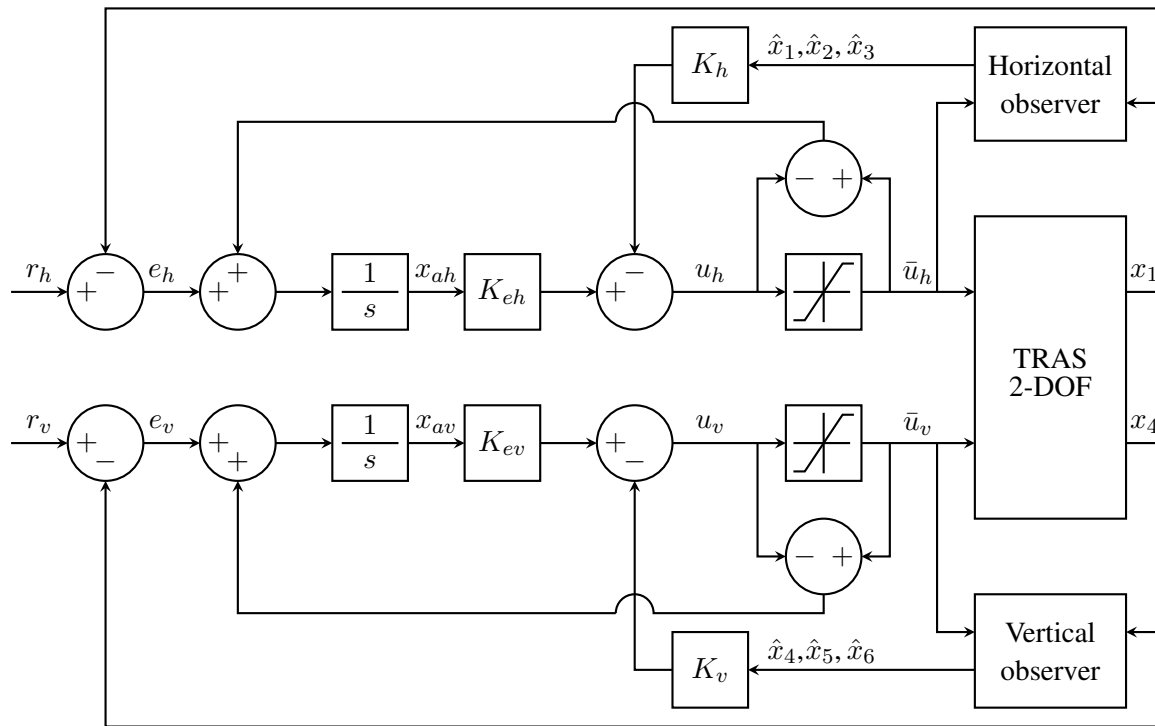


Fig. 4 TRAS with decoupled integral LQR controller (DILQRC), full state observer and back-calculation technique.

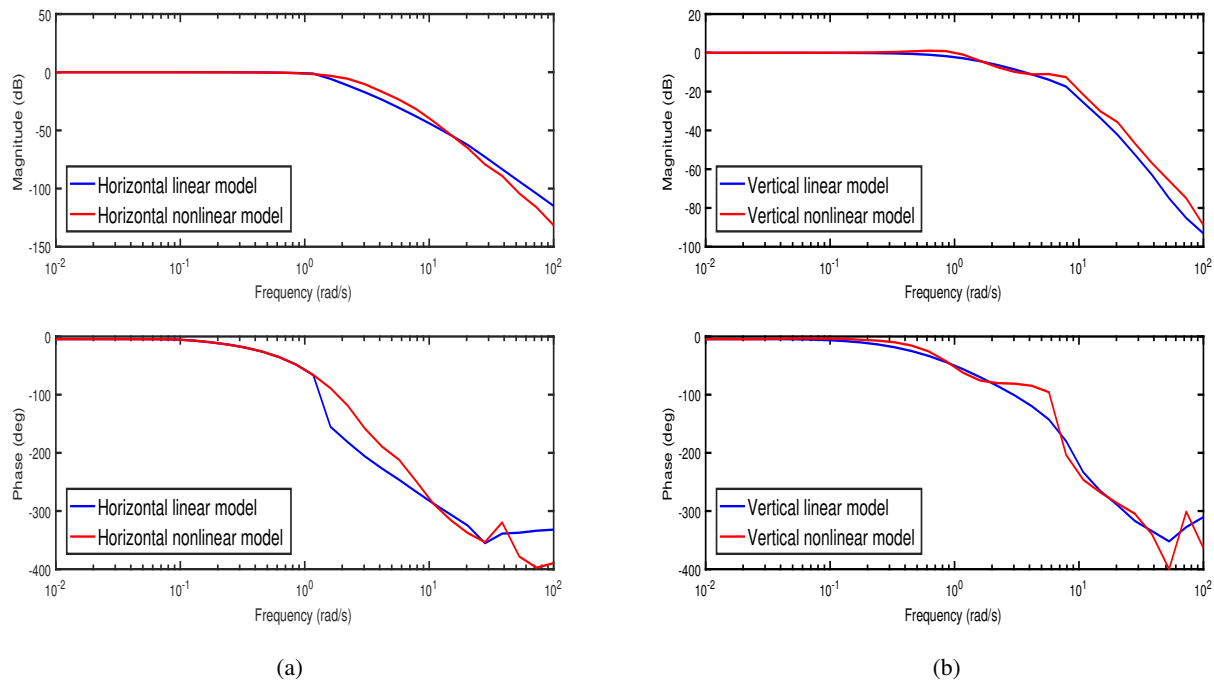


Fig. 5 Estimated frequency response of each closed loop subsystem. (a) Horizontal subsystem , (b) Vertical subsystem.

## 8 Simulation Results

The performance of the closed loop system is depending on the transient response of the system, error, control and total variation indices. For assessing the transient response characteristic, the rise time ( $RT$ ) is defined as the time it takes for the response to rise from 10% to 90% of the steady state value, the settling time ( $ST$ ) is defined as the time it takes for the response to fall within 5% of the steady state value and the percentage of the overshoot ( $OV$ ) as the the maximum peak value of the response expressed as a percentage of the steady state value [18]. Error index is defined as the integrated absolute of error ( $IAE$ ) between the reference signal and the controlled variable and is given as in Eq. 36 [23]:

$$IAE = \int_0^{\infty} |e(t)| dt \quad (36)$$

where:  $e(t)$  is the difference between the reference signal and the controlled variable.

The control index is defined as the integrated absolute control signal ( $IAC$ ) that determines the amount of the control effort produced by the controller and is given as in Eq. 37 [23]:

$$IAC = \int_0^{\infty} |u(t)| dt \quad (37)$$

where:  $u(t)$  is the control signal.

The total variation ( $TV$ ) index characterise the smoothness of the control signal and input usage and is given as in Eq. 38 [8]:

$$TV = \sum_{m=1}^{n_s} |u_i(m+1) - u_i(m)| \quad (38)$$

where:  $n_s$  is the number of samples and  $u_i(1), u_i(2), \dots, u_i(n_s)$  is the discretised sequence of the input signals.

Lower indices indicate accurate tracking for the reference signal, less control effort and less aggressive changes in control signal, respectively. The closed loop system is implemented in MATLAB/Simulink using ode5 solver with a fixed step size of 0.01 s. For testing purpose, a nonlinear 2-DOF TRAS model given in [13] is considered in this study for the evaluation of the designed controller performance.

### 8.1 Set Point Tracking

In this sub-section, simulation results of decoupled integral LQR controller (DILQRD) and cross coupled

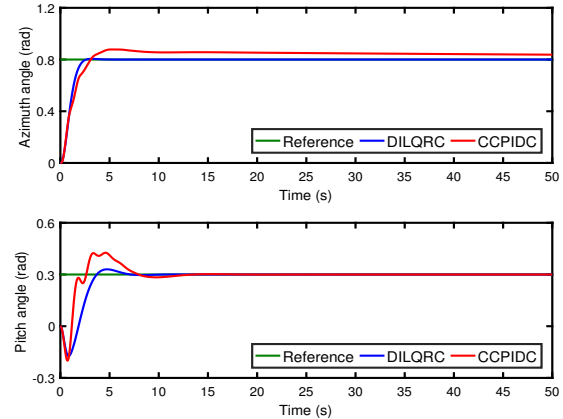


Fig. 6 Step input response of TRAS with DILQRC and CCPIDC.

**Table 3** Step reference performance characteristics.

| Controller  | Plane      | $RT(s)$ | $ST(s)$ | $OV(\%)$ |
|-------------|------------|---------|---------|----------|
| CCPIDC [13] | Horizontal | 2.07    | 44.77   | 9.75     |
|             | Vertical   | 0.49    | 7.02    | 42.06    |
| DILQRC      | Horizontal | 1.39    | 2.02    | 0.70     |
|             | Vertical   | 1.37    | 5.44    | 10.02    |

PID controller (CCPIDC) for set point tracking are discussed and compared. Figure 6 shows the response of the TRAS system due to step input of 0.8 rad in horizontal plane and 0.3 rad in vertical plane with both DILQRC and CCPIDC. Table 3 summaries the step reference performance characteristics of DILQRC and CCPIDC. For the horizontal plane the DILQRC achieves better performance by reducing the rise time by 32.85%, the settling time by 95.49% and the percentage of overshoot by 92.82% as compared to the CCPIDC. For the vertical plane the CCPIDC has a better rise time than the DILQRC, meanwhile, it takes 7.02 seconds to be settled, whereas the DILQRC takes only 5.44 seconds to be settled with magnificent reduction in overshoot percentage from 42.06% to 10.02% as compared to CCPIDC.

Figure 7 shows the input control signal of DILQRC and CCPIDC due to step input. The error, control and total variation indices of DILQRC and CCPIDC due to step input are summarised in Table 4. It can be clearly observed that the DILQRC reduces the error index for both planes indicating accurate tracking for the reference signal with less control effort and less aggressive changes in the control signal as compared to the CCPIDC.

Figure 8 shows the response of the TRAS system due to square wave input with amplitude of 0.8

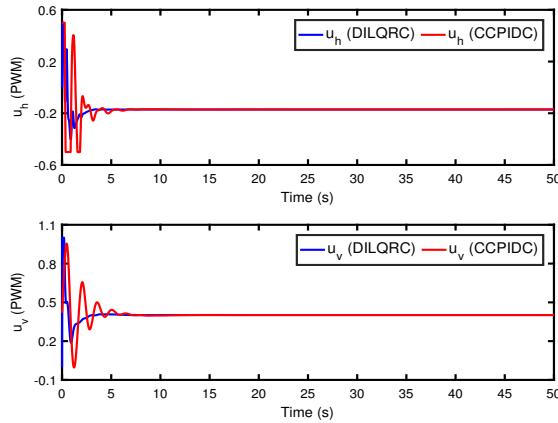


Fig. 7 Control signal of DILQRC and CCPIDC due to step input.

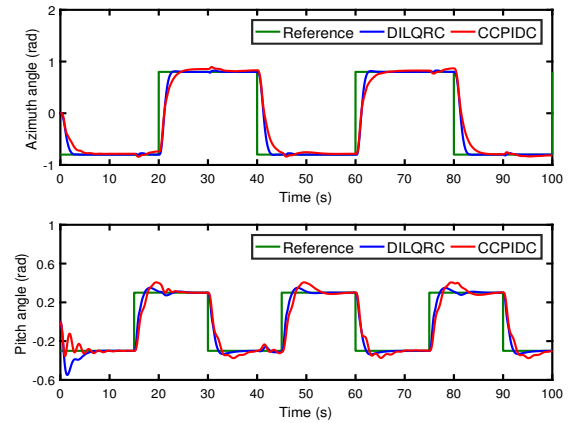


Fig. 8 Square-wave response of TRAS with DILQRC and CCPIDC.

**Table 4** Error, control and total variation indices of DILQRC and CCPIDC due to step input.

| Controller  | Plane      | IAE  | IAC   | TV   |
|-------------|------------|------|-------|------|
| CCPIDC [13] | Horizontal | 3.30 | 9.00  | 3.68 |
|             | Vertical   | 1.04 | 20.33 | 3.00 |
| DILQRC      | Horizontal | 0.82 | 8.75  | 2.76 |
|             | Vertical   | 1.03 | 20.14 | 2.06 |

rad and frequency of 0.025 Hz in horizontal plane and square wave input with amplitude of 0.3 rad and frequency of 0.03Hz in vertical plane for both DILQRC and CCPIDC.

Figure 9 shows the input control signal of DILQRC and CCPIDC due to square wave input. Table 5 summaries the error, control and total variation indices for DILQRC and CCPIDC due to square wave input signal. It can be clearly observed that the DILQRC produces high control effort with more aggressive changes in the control signal as compared to the CCPIDC. On the other side, the DILQRC maintains accurate tracking for the reference signal by reducing the error index of horizontal and vertical angles by 32.05% and 31.66%, respectively.

**Table 5** Error, control and total variation indices of DILQR and CCPIDC due to square wave input.

| Controller  | Plane      | IAE   | IAC   | TV    |
|-------------|------------|-------|-------|-------|
| CCPIDC [13] | Horizontal | 13.98 | 16.20 | 27.21 |
|             | Vertical   | 7.17  | 28.05 | 22.33 |
| DILQRC      | Horizontal | 9.50  | 16.54 | 35.76 |
|             | Vertical   | 4.90  | 28.88 | 28.70 |

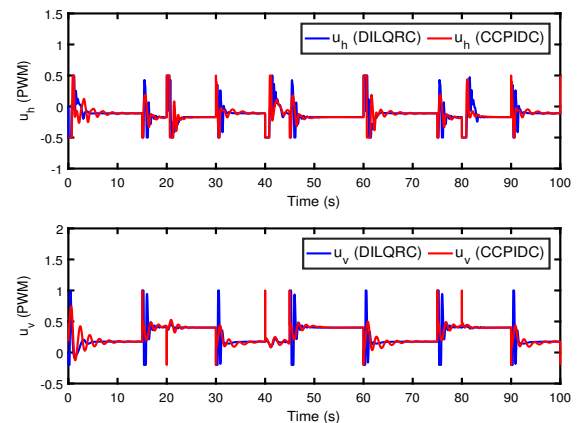


Fig. 9 Control signal of DILQRC and CCPIDC due to square wave input.

## 8.2 Disturbance Rejection

To examine the ability of each controller to reject the disturbance and maintain accurate tracking for the reference signal an external step input disturbance of 0.2 rad is injected to the system in both planes at time 25 seconds as shown in Figure 10. It can be noticed that the DILQRC rejects the disturbance very fast and maintains accurate tracking for the reference signal in both planes as compared to the CCPIDC.

Figure 11 shows the input control signal of DILQRC and CCPIDC due to step input subjected to external disturbance. Table 6 summaries the error, control and total variation indices for each controller with step input subjected to external disturbance. It can be observed that the the DILQRC requires slightly higher control effort to stabilise both planes of the system with more aggressive changes in the control signal as com-

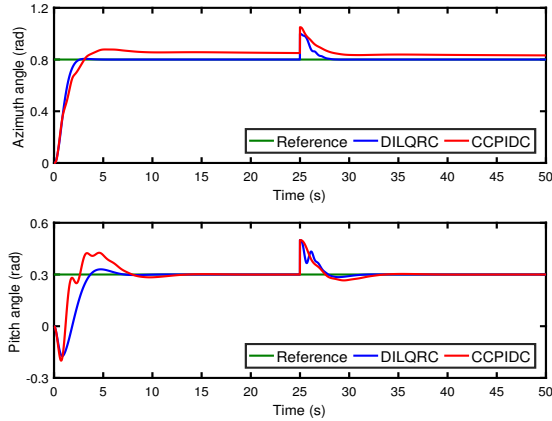


Fig. 10 Step input response of TRAS with DILQRC and CCPIDC subjected to external disturbance.

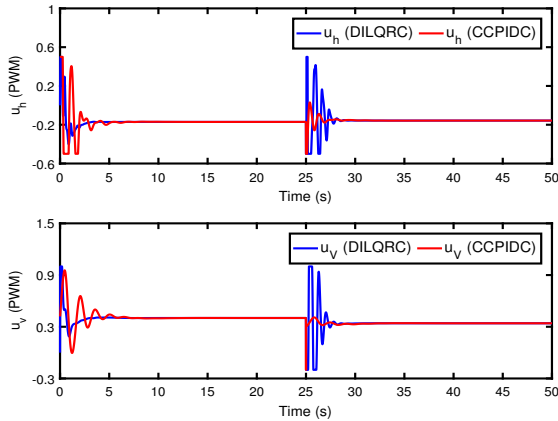


Fig. 11 Control signal of DILQRC and CCPIDC due to step input subjected to external disturbance.

pared to CCPIDC. In terms of error index, the DILQRC achieves better performance by rejecting the disturbance very fast and maintains accurate tracking for the reference signal by reducing the error index by 68.91% and 7.14% for horizontal and vertical planes, respectively as compared to the CCPIDC.

## 9 Experimental Results

A successful validation of the proposed control strategy is validated through experimental results with real TRAS system in 2-DOF, the experimental validation is based on set point tracking and disturbance rejection of both DILQRC and CCPIDC.

**Table 6** Error, control and total variation indices of DILQRC and CCPIDC due to step input subjected to external disturbance.

| Controller  | Plane      | IAE  | IAC   | TV   |
|-------------|------------|------|-------|------|
| CCPIDC [13] | Horizontal | 3.41 | 8.66  | 5.15 |
|             | Vertical   | 1.40 | 18.80 | 4.37 |
| DILQRC      | Horizontal | 1.06 | 8.74  | 8.68 |
|             | Vertical   | 1.30 | 18.85 | 7.72 |

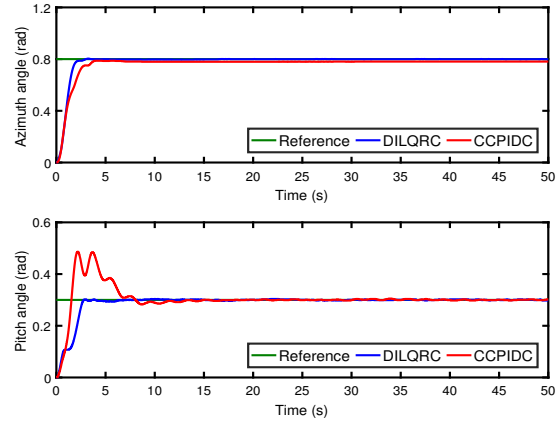


Fig. 12 Step input response of TRAS with DILQRC and CCPIDC.

### 9.1 Set Point Tracking

For the step set point tracking the system is subjected to step input of 0.8 rad in horizontal plane and 0.3 rad in vertical plane. Figure 12 shows the response of the TRAS system due to step input with both DILQRC and CCPIDC. Table 7 summaries the step reference performance characteristics of DILQRC and CCPIDC. For the horizontal plane the DILQRC achieves better performance than the CCPIDC by reducing the rise time by 39.60% and the settling time by 46.49%. For the vertical plane the CCPIDC has a better rise time than the DILQRC but it takes 8.90 seconds to be settled, whereas the DILQRC takes only 2.60 seconds with magnificent reduction in overshoot percentage from 62.09% to 1.24%.

Figure 13 shows the input control signal of

**Table 7** Step reference performance characteristics.

| Controller  | Plane      | RT(s) | ST(s) | OV(%) |
|-------------|------------|-------|-------|-------|
| CCPIDC [13] | Horizontal | 2.02  | 3.42  | 0.00  |
|             | Vertical   | 1.08  | 8.90  | 62.09 |
| DILQRC      | Horizontal | 1.22  | 1.83  | 0.48  |
|             | Vertical   | 2.16  | 2.60  | 1.24  |

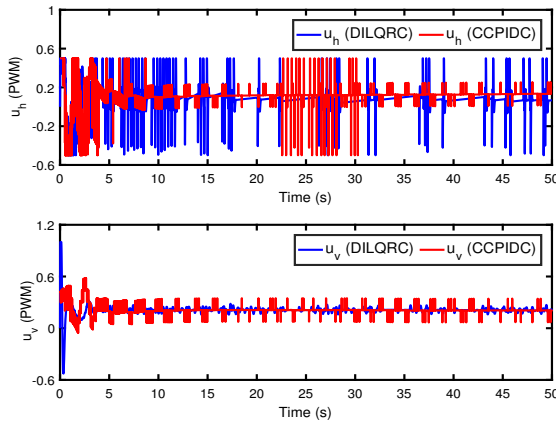


Fig. 13 Control signal of DILQRC and CCPIDC due to step input.

**Table 8** Error, control and total variation indices of DILQRC and CCPIDC due to step input.

| Controller  | Plane      | IAE  | IAC   | TV     |
|-------------|------------|------|-------|--------|
| CCPIDC [13] | Horizontal | 1.96 | 7.29  | 201.52 |
|             | Vertical   | 0.97 | 10.86 | 87.58  |
| DILQRC      | Horizontal | 0.89 | 6.34  | 145.52 |
|             | Vertical   | 0.52 | 10.81 | 16.93  |

DILQRC and CCPIDC due to step input. The error, control and total variation indices of DILQRC and CCPIDC due to step input are summarised in Table 8. It can be clearly observed that the DILQRC significantly reduces the error index by 54.59% and 46.39% for horizontal and vertical planes, respectively indicating accurate tracking for the reference signal with less control effort and less aggressive changes in the control signal as compared to the CCPIDC.

Figure 14 shows the response of the TRAS system due to square wave input with amplitude of 0.8 rad and frequency of 0.025 Hz in horizontal plane and square wave input with amplitude of 0.3 rad and frequency of 0.03Hz in vertical plane with both DILQRC and CCPIDC. It can be clearly observed that the DILQRC accurately tracks the reference signal in both planes with reduced number of oscillation in vertical plane as compared to the CCPIDC.

Figure 15 shows the input control signal of DILQRC and CCPIDC due to square wave input. Table 9 summaries the error, control and total variation indices for DILQRC and CCPIDC due to square wave input signal . It can be observed that the the DILQRC requires less control effort to stabilise the horizontal plane with less aggressive changes in control signal as compared to CCPIDC. For the vertical plane the DILQRC

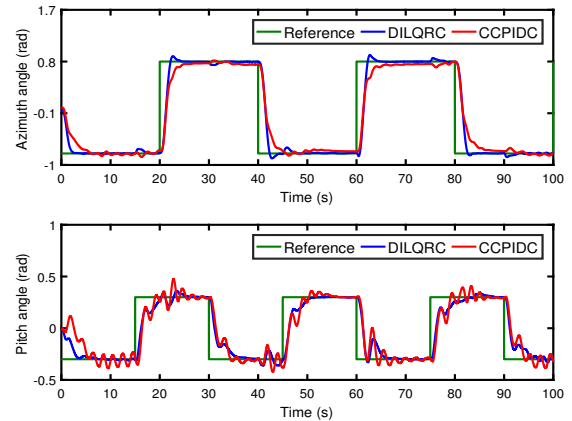


Fig. 14 Square-wave response of TRAS with DILQRC and CCPIDC.

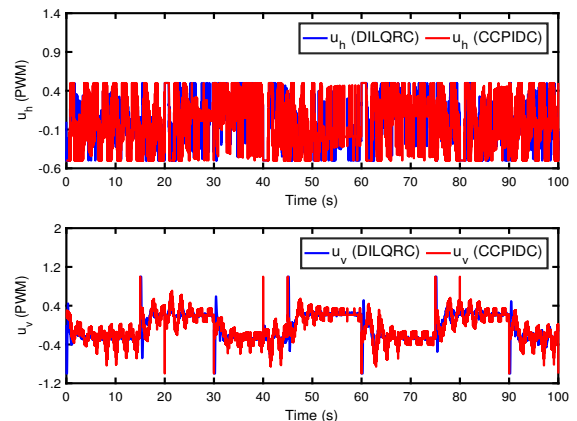


Fig. 15 Control signal of DILQRC and CCPIDC due to square-wave input.

requires higher control effort to stabilise the system with less aggressive changes in control signal as compared to CCPIDC. In terms of error index, the DILQRC achieves better performance by maintaining accurate tracking for the reference signal by reducing the error index by 28.57% and 24.40% for horizontal and vertical planes, respectively as compared to the CCPIDC. In addition, it can be noticed that the CCPIDC produce high frequency control signal due to the presence of the differential part of the controller, which results in more aggressive changes in the control signal.

## 9.2 Disturbance Rejection

With the presence of environmental disturbances on real laboratory TRAS system, an external step input disturbance of 0.2 rad is injected in both planes of the system at time 25 seconds. The performance of DILQRC

**Table 9** Error, control and total variation indices of DILQRC and CCPIDC due to square-wave input.

| Controller  | Plane      | <i>IAE</i> | <i>IAC</i> | <i>TV</i> |
|-------------|------------|------------|------------|-----------|
| CCPIDC [13] | Horizontal | 15.76      | 25.09      | 2050.10   |
|             | Vertical   | 10.49      | 24.64      | 725.29    |
| DILQRC      | Horizontal | 11.25      | 22.66      | 756.96    |
|             | Vertical   | 7.93       | 25.15      | 66.44     |

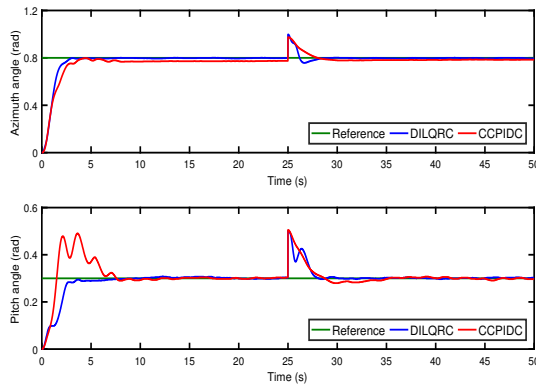


Fig. 16 Step input response of TRAS with DILQRC and CCPIDC subjected to external disturbance.

and CCPIDC is recorded and compared as shown in Figure 16. It can be noticed that the DILQRC rejects the disturbance very fast and maintains accurate tracking for the set point in both planes as compared to the CCPIDC.

Figure 17 shows the input control signal of DILQRC and CCPIDC due to step input subjected to external disturbance. Table 10 summaries the error, control and total variation indices of DILQRC and CCPIDC subjected to external disturbance. It can be observed that the the DILQRC requires higher control effort to stabilise both planes of the system with less aggressive changes in control signal as compared to CCPIDC. In terms of error index, the DILQRC achieves better performance by rejecting the disturbance very fast and maintains accurate tracking for the reference signal by reducing the error index by 47.27% and 34.35% for horizontal and vertical planes, respectively as compared to the CCPIDC.

## 10 Conclusion

In this work, control and stabilisation of the nonlinear TRAS system in 2-DOF motion is successfully achieved. Decoupled integral LQR controller combined with full state observer and anti-integral windup com-

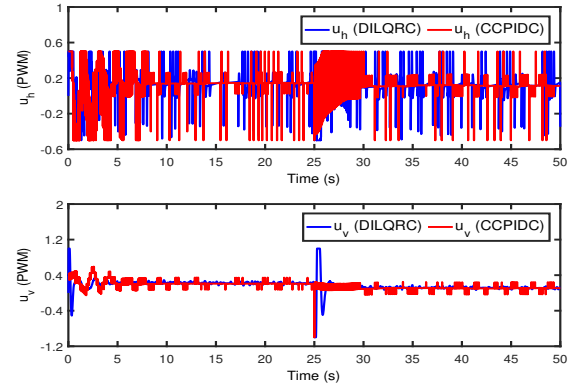


Fig. 17 Control signal of DILQRC and CCPIDC due to step input subjected to external disturbance.

**Table 10** Error, control and total variation indices of DILQRC and CCPIDC due to step input subjected to external disturbance.

| Controller  | Plane      | <i>IAE</i> | <i>IAC</i> | <i>TV</i> |
|-------------|------------|------------|------------|-----------|
| CCPIDC [13] | Horizontal | 2.20       | 7.49       | 416.03    |
|             | Vertical   | 1.31       | 8.22       | 126.60    |
| DILQRC      | Horizontal | 1.16       | 8.60       | 199.71    |
|             | Vertical   | 0.86       | 9.37       | 21.81     |

pensator based on back-calculation technique has been described in this paper. Simulation and experimental results show that the DILQRC has a better transient and steady state responses with magnificent reduction of settling time, overshoot percentage and error index also it requires less and smooth control signal in case of tracking a step input as compared to the CCPIDC. In all the experiments, the DILQRC produces a smooth control signal with less aggressive changes as compared to the CCPIDC, furthermore, the settling time for the system is less than 2.61 seconds for both angles, which is considered as the fastest settling time as compared to the other controller design techniques presented in the literature. Overall, the DILQRC has the ability of maintaining accurate tracking for the reference signal with fast disturbance rejection as compared to the existing CCPIDC tuned by the manufacturer.

## 11 Acknowledgement

The authors would like to acknowledge the UTM-GUP Grant from Universiti Teknologi Malaysia (UTM) and Malaysian Government with vote number 17H40 for supporting this work.

## References:

- [1] Salman Ijaz, Mirza Tariq Hamayun, Lin Yan, and Muhammad Faisal Mumtaz. Fractional order modeling and control of twin rotor aero dynamical system using nelder mead optimization. *Journal of Electrical Engineering and Technology*, 11(6):1863–1871, 2016.
- [2] Xiaoyan Yang, Jianwei Cui, Dazhong Lao, Donghai Li, and Junhui Chen. Input shaping enhanced active disturbance rejection control for a twin rotor multi-input multi-output system (trms). *ISA transactions*, 62:287–298, 2016.
- [3] Mashhood Ahmad, Ahsan Ali, and Mohammad Ahmad Choudhry. Fixed-structure  $H_\infty$  controller design for two-rotor aerodynamical system (tras). *Arabian Journal for Science and Engineering*, 41(9):3619–3630, 2016.
- [4] Ayad Al-Mahturi and Herman Wahid. Optimal tuning of linear quadratic regulator controller using a particle swarm optimization for two-rotor aerodynamical system. *World Academy of Science, Engineering and Technology, International Journal of Electrical, Computer, Energetic, Electronic and Communication Engineering*, 11(2):196–202, 2017.
- [5] A. Phillips and F. Sahin. Optimal control of a twin rotor mimo system using lqr with integral action. In *2014 World Automation Congress (WAC)*, pages 114–119, Aug 2014.
- [6] Sumit Kumar Pandey and Vijaya Laxmi. Optimal control of twin rotor mimo system using lqr technique. In *Computational Intelligence in Data Mining-Volume 1*, pages 11–21. Springer, 2015.
- [7] Peng Wen and T-W Lu. Decoupling control of a twin rotor mimo system using robust deadbeat control technique. *IET Control Theory & Applications*, 2(11):999–1007, 2008.
- [8] Vinay Kumar Pandey, Indrani Kar, and Chitralekha Mahanta. Controller design for a class of nonlinear mimo coupled system using multiple models and second level adaptation. *ISA transactions*, 69:256–272, 2017.
- [9] Saif S Butt and Harald Aschemann. Multi-variable integral sliding mode control of a two degrees of freedom helicopter. *IFAC-PapersOnLine*, 48(1):802–807, 2015.
- [10] Dan-Adrian Duțescu, Mircea-Bogdan Radac, and Radu-Emil Precup. Model predictive control of a nonlinear laboratory twin rotor aero-dynamical system. In *Applied Machine Intelligence and Informatics (SAMi), 2017 IEEE 15th International Symposium on*, pages 000037–000042. IEEE, 2017.
- [11] R. Raghavan and S. Thomas. MIMO model predictive controller design for a twin rotor aerodynamic system. In *2016 IEEE International Conference on Industrial Technology (ICIT)*, pages 96–100, March 2016.
- [12] A. Haruna, Z. Mohamed, M. Ö. Efe, and Mohd Ariffanan M. Basri. Dual boundary conditional integral backstepping control of a twin rotor mimo system. *Journal of the Franklin Institute*, 354(15):6831 – 6854, 2017.
- [13] INTECO. *Two Rotor Aero-Dynamical System User's Manual*, 2013.
- [14] H.K. Khalil. *Nonlinear Systems*. Pearson Education. Prentice Hall, 2002.
- [15] N.S. Nise. *Control Systems Engineering*. Wiley, 2011.
- [16] Elumalai Vinodh Kumar, Ganapathy Subramanian Raaja, and Jovitha Jerome. Adaptive pso for optimal lqr tracking control of 2 dof laboratory helicopter. *Applied Soft Computing*, 41:77–90, 2016.
- [17] J Hamidi. Control system design using particle swarm optimization (pso). *International Journal of Soft Computing and Engineering*, 1(6):116–119, 2012.
- [18] K. Ogata. *Modern Control Engineering*. Prentice Hall, 2010.
- [19] SM Ahmad, AJ Chipperfield, and O Tokhi. Dynamic modeling and optimal control of a twin rotor mimo system. In *National Aerospace and Electronics Conference, 2000. NAECON 2000. Proceedings of the IEEE 2000*, pages 391–398. IEEE, 2000.
- [20] Antonio Visioli. Anti-windup strategies. *Practical PID control*, pages 35–60, 2006.
- [21] Jong-Woo Choi and Sang-Cheol Lee. Antiwindup strategy for pi-type speed controller. *IEEE Transactions on Industrial Electronics*, 56(6):2039–2046, 2009.
- [22] Karl Johan Astrom and Lars Rundqwist. Integrator windup and how to avoid it. In *American Control Conference, 1989*, pages 1693–1698. IEEE, 1989.
- [23] Andrzej Pawlowski, Carlos Rodríguez, José Luis Guzmán, Manuel Berenguel, and Sebastián Dormido. Measurable disturbances compensation: Analysis and tuning of feedforward techniques for dead-time processes. *Processes*, 4(2):12, 2016.